

ADVANCED MATERIALS

Supporting Information

for *Adv. Mater.*, DOI: 10.1002/adma.201704378

A Li–Air Battery with Ultralong Cycle Life in Ambient Air

*Lie Wang, Jian Pan, Ye Zhang, Xunliang Cheng, Lianmei Liu,
and Huisheng Peng**

Supporting Information

Experimental Section

Materials. Lithium metal were obtained from China Energy Lithium Co., Ltd. Lithium triflate ($\text{CF}_3\text{SO}_3\text{Li}$, 98%). Tetraethylene glycol dimethyl ether ($\text{C}_{10}\text{H}_{22}\text{O}_5$, 99%), and N-methyl-2-pyrrolidinone ($\text{C}_5\text{H}_9\text{NO}$, 99%) were purchased from Aladdin Reagent. Lithium iodide (LiI, 99.9%), trimethylolpropane ethoxylate triacrylate (average M_n of ~ 428), 2-hydroxy-2-methyl-1-phenyl-1-propanone ($\text{C}_6\text{H}_5\text{COC}(\text{CH}_3)_2\text{OH}$, 97%), poly(vinylidene fluoride-co-hexafluoropropylene) (average M_n of ~ 130000) and lithium peroxide (Li_2O_2 , 90%) were provided by Sigma-Aldrich. Low-density polyethylene (LDPE) film was obtained from Taizhou Yuzhu Household Products Co. Ltd.

Synthesis of the spinnable carbon nanotube array. Spinnable carbon nanotube (CNT) arrays were synthesized by chemical vapor deposition with Fe (1.1 nm)/ Al_2O_3 (3 nm) on a silicon substrate as the catalyst. Ethylene with a flowing rate of 90 sccm was used as the carbon source, and a gas mixture of argon (400 sccm) and hydrogen (30 sccm) was used as the carrier gas. The growth occurred at 740 °C for 10 min. The highly aligned CNT sheets were continuously drawn out of the spinnable CNT array.

Preparation of the gel electrolyte. At the first step, a precursor solution of gel electrolyte was obtained by mixing Solutions A, B and C. Here, the Solution A was prepared by dissolving 0.318 g lithium triflate in 2.018 g tetraethylene glycol dimethyl ether. Solution B was prepared by dissolving 0.584 g poly (vinylidene fluoride-co-hexafluoropropylene) in 2.336 g N-methyl-2-pyrrolidinone. Solution C was obtained by adding 0.006 g 2-hydroxy-2-methyl-1-phenyl-1-propanone to 1.752 g trimethylolpropane ethoxylate triacrylate. Then, the precursor solution was cast on a glass substrate, followed by a 365 nm UV irradiation for about 10 s to produce a solid gel electrolyte. In order to obtain the gel electrolyte containing a redox mediator, the as-obtained gel electrolyte was immersed in a Solution D for 12 h. Here, the Solution D was prepared by dissolving 0.067 g lithium iodide and 1.59 g lithium triflate in 10 mL of tetraethylene glycol dimethyl ether. All samples were prepared in an argon-filled glove box. Solution C and the precursor solution were stored in darkness.

Fabrication of the Li-air battery. The air electrode was prepared by stacking 20 layers of CNT sheets. Li sheet, gel electrolyte, air electrode and LDPE film were assembled in sequence in Swagelok-type Li-air battery.

Fabrication of the flexible fiber-shaped Li-air battery. A Li wire connected with a copper wire current collector was dipped into the precursor solution, followed by exposing to UV irradiation for about 10 s in an argon-filled glove box. The process was repeated for at least three times. Then, the gel electrolyte-coated Li wire was immersed in a Solution D for 12 h. After that, the aligned CNT sheets were carefully wrapped with the air electrode, followed by wrapping a layer of LDPE film. A punched heat-shrinkable tube was finally used to protect the resulting Li-air battery.

Fabrication of the flexible strap-shaped Li-air battery. The strap-shaped Li-air battery was assembled with punched aluminum plastic film as the package material. A CNT sheet and a Li foil were separated by a gel electrolyte. Before package, a layer of LDPE film was placed at the top of the CNT sheet.

Electrochemical measurements. The electrochemical measurements were conducted on an Arbin multichannel electrochemical testing system (MSTAT-5 V/10 mA/16Ch). The specific capacity (C) was calculated by $C = (I \times t) / m$, where I , t , and m represent the discharge current, discharge time, and weight of the air electrode, respectively. All test procedures were conducted in the ambient air.

Characterization. The structures were characterized by scanning electron microscope (SEM, Hitachi FE-SEM S-4800 operated at 1 kV), transmission electron microscopy (TEM, JEOL, JEM-2100F), X-ray diffraction (XRD, Bruker AXS D8), and Fourier transform infrared spectrum (FTIR, NICOLET 6700). X-ray photoelectron spectroscopy (XPS) was recorded on an AXIS ULTRA DLD XPS System with MONO Al source (Shimadzu Corp.). Photoelectron spectrometer was recorded by using monochromatic Al KR radiation under vacuum at 5×10^{-9} Pa. The N_2 adsorption isotherms and specific surface area were determined using an automated surface area and pore size analyzer (QUADRASORB *SI*). The photographs were taken by a camera (Nikon, J1). The O_2 and CO_2 permeability value of the LDPE film was measured by pressure difference method according to GB/T 1038-2000 criterion, which was commissioned testing by the third party institution. Permeability values were typically reported in Barrer units ($1 \text{ Barrer} = 1 \times 10^{-10} \text{ cm}^3 \text{ (STP) cm cm}^{-2} \text{ s}^{-1} \text{ cm Hg}^{-1} = 3.348 \times 10^{-16} \text{ mol m m}^{-2} \text{ Pa}^{-1} \text{ s}^{-1}$). The H_2O permeability value test of the LDPE film was performed according to ASTM E96 inverse cup standard. The H_2O permeability value was determined on the basis of the equation: H_2O permeability value = $24 \times (W_2 - W_1) / (S \times t)$, where the unit of H_2O permeability value is $\text{g m}^{-2} \text{ d}^{-1}$, $W_2 - W_1$ is the mass variation of distilled water during testing, S is the area of the samples and t is the testing time.

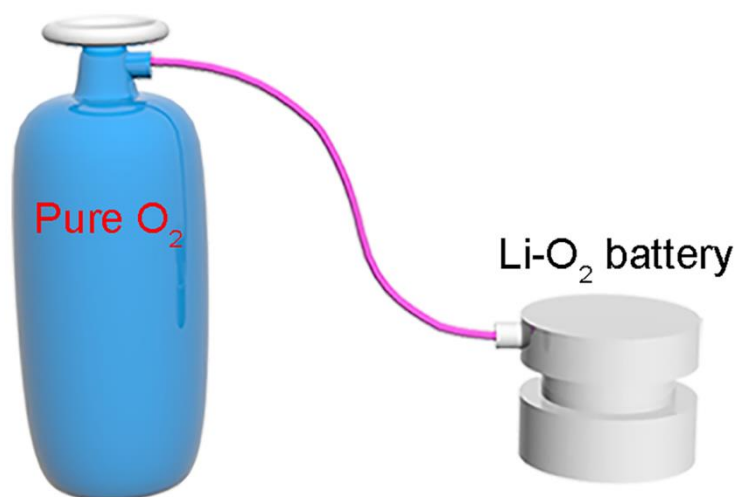


Figure S1. Schematic illustration to a conventional Li-air (Li-O₂) battery that works in pure O₂ atmosphere.

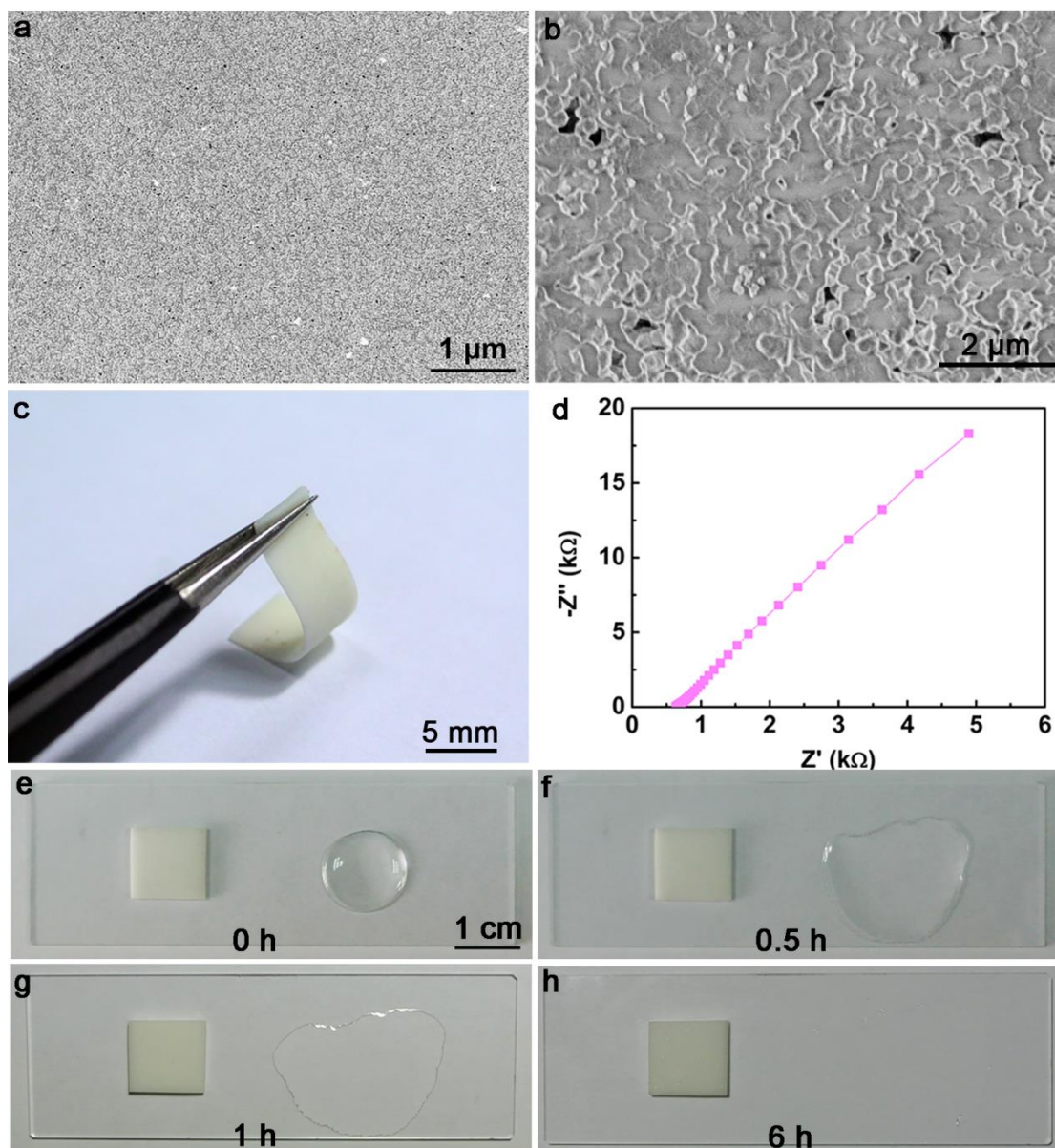


Figure S2. SEM images of the gel electrolyte in **a)** low and **b)** high magnifications. **c)** Photograph of a gel electrolyte under bending. **d)** Electrochemical impedance spectroscopy (EIS) of the gel electrolyte at the frequency range of 1 Hz to 100 kHz. The ionic conductivity (s) of gel electrolyte was calculated from the equation of $s = l/(R \times A)$, where l , R , and A correspond to the thickness, resistance, and area of gel electrolyte, respectively. **e-h)** The comparison of gel electrolyte (left) and liquid electrolyte (right) exposed in air for 6 h.

Figures S2a and b present typical SEM images of the gel electrolyte that was uniform and formed an interconnected porous structure to favor lithium ion transfer between the cathode and the anode. The gel electrolyte was flexible with high bendability and mechanical stability (Figure S2c). Moreover, a high ionic conductivity of 2.52 mS

cm^{-1} was obtained (Figure S2d), which is approached to that of liquid electrolyte. The gel electrolyte also showed a higher stability and safety than liquid electrolyte in an open air system. As shown in Figures S2e-h, a gel electrolyte and a liquid electrolyte with equal mass were exposed in ambient air. The gel electrolyte remained almost unchanged after 6 h, while the liquid electrolyte easily flowed and volatilized.

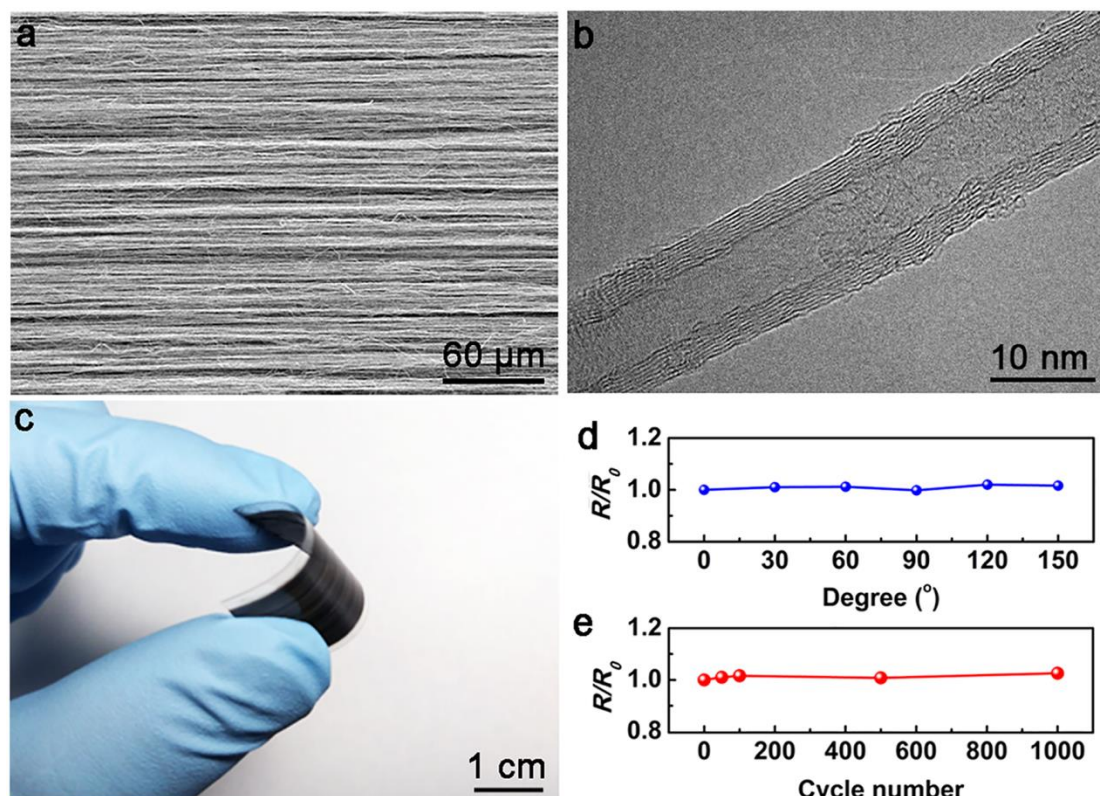


Figure S3. a) SEM image of the aligned CNT air electrode. b) TEM image of a CNT. c) Photograph of an aligned CNT air electrode being bent into a curved structure. Dependence of electrical resistance of aligned CNT air electrode on d) bending angle and e) bending cycle at a bending angle of 90°. Here R and R_0 correspond to the electrical resistances before and after bending, respectively.

Figure S3a shows SEM images of a typical aligned CNT air electrode where CNTs were highly aligned along the length direction. The CNT showed a multi-walled structure with diameter of ~12 nm (Figure S3b), and the formed aligned micro- and nano-scale pores among the CNTs favored an efficient diffusion of O_2 and a uniform formation of discharge product, so they may serve as an excellent reactor for Li-air batteries. Moreover, the aligned CNT air electrode was lightweight and flexible (Figure S3c), and the resistance can be well maintained under bending with increasing angles and repeated bending cycles (Figures S3d and e).



Figure S4. Photograph of the LDPE film.

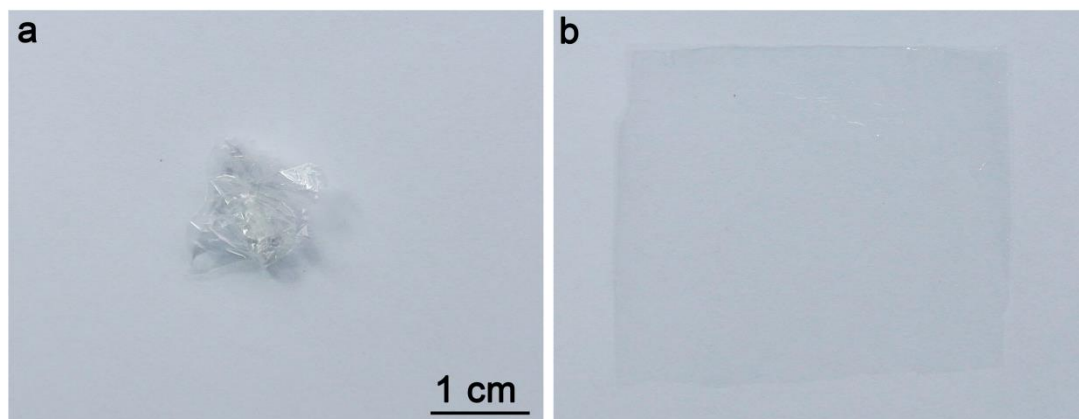


Figure S5. Photographs of an LDPE film that shrunk into a ball **a)** and was paved again **b)**.

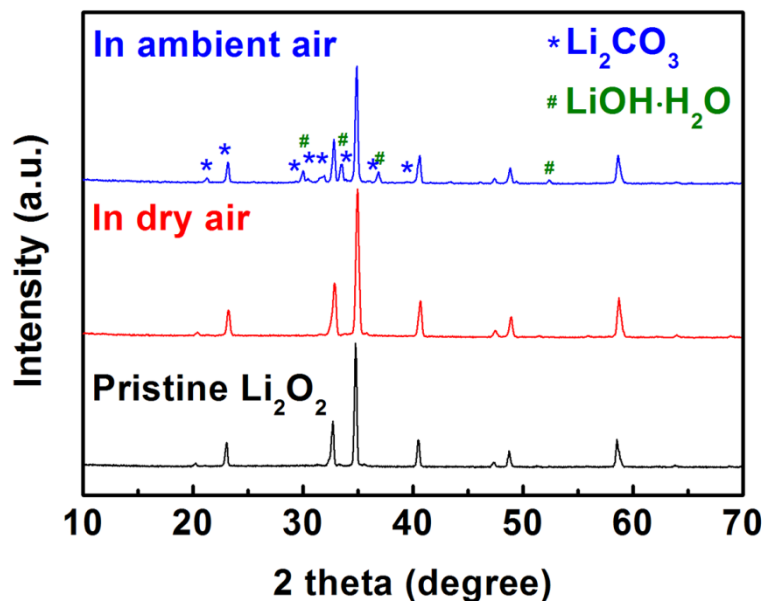


Figure S6. XRD patterns of pristine Li_2O_2 and Li_2O_2 in ambient air and dry air after 1 day.

Figure S6 shows the effect of moisture on the stability of Li_2O_2 in ambient air. The Li_2O_2 powder remained stable in dry air after 1 day, while it turned into LiOH and Li_2CO_3 quickly in ambient air. Therefore, the moisture in ambient air can accelerate the transformation of Li_2O_2 to LiOH and Li_2CO_3 . In our Li-air batteries, the use of LDPE film can restrain the permeation of moisture from air, which can therefore restrain the side reactions of discharge product of Li_2O_2 to LiOH and Li_2CO_3 in ambient air (Figure 1c).



Figure S7. Photograph of the comparison between Li_2O_2 powders with (right) and without (left) the protection of LDPE film in ambient air for 3 days.

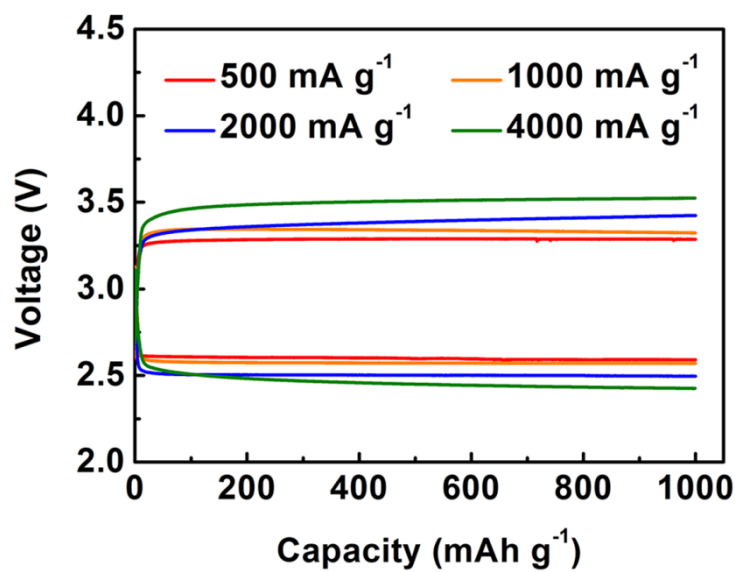


Figure S8. Rate performance of the Li-air battery at different current densities in ambient air (relative humidity of ~50%).

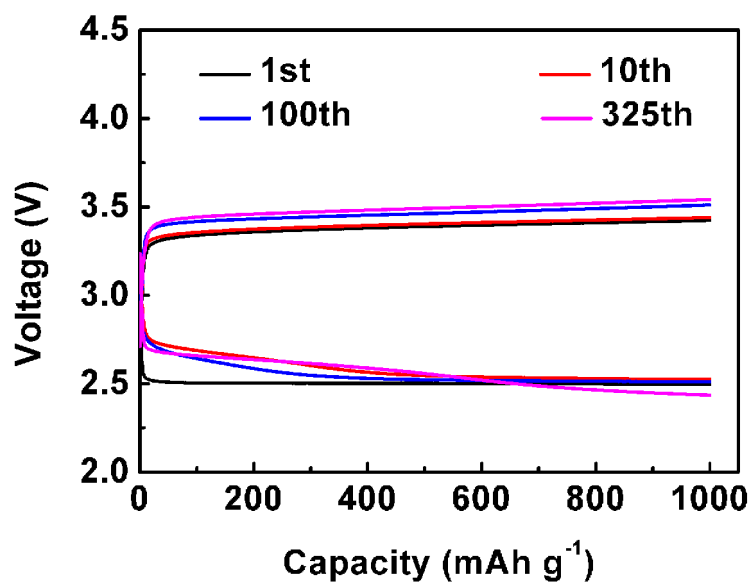


Figure S9. Cycle performance of the Li-air battery with LDPE film and LiI in ambient air (relative humidity of ~50%).

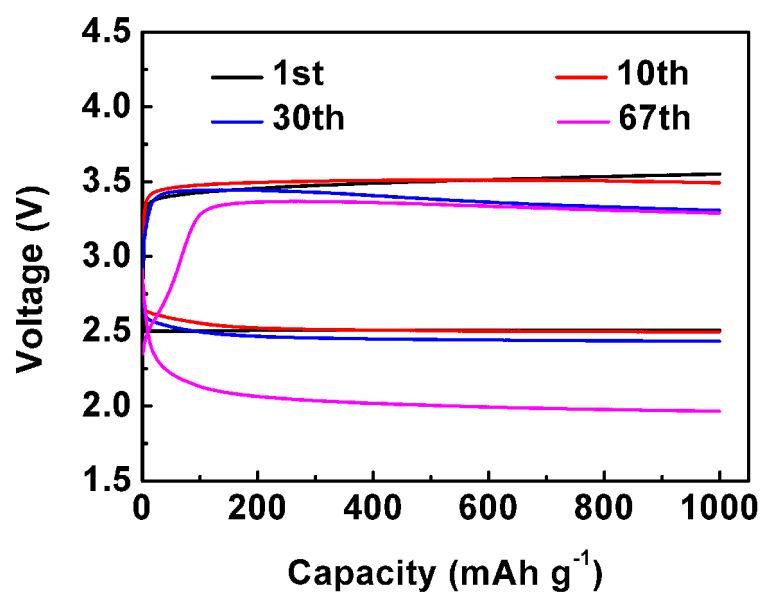


Figure S10. Cycle performance of the Li-air battery with LiI but without LDPE film in ambient air (relative humidity of ~50%).

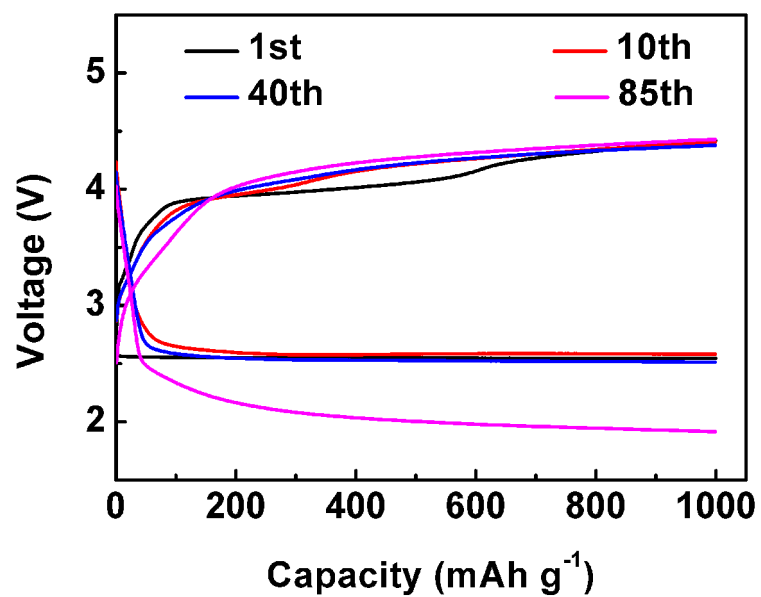


Figure S11. Cycle performance of the Li-air battery with LDPE film but without LiI in ambient air (relative humidity of ~50%).

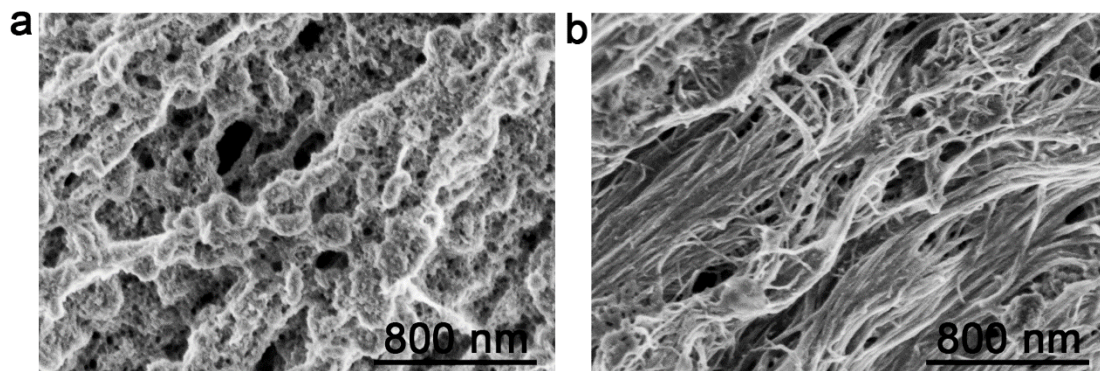


Figure S12. SEM images of the air electrode after the 300th (a) discharging and (b) recharging in ambient air with LDPE and LiI.

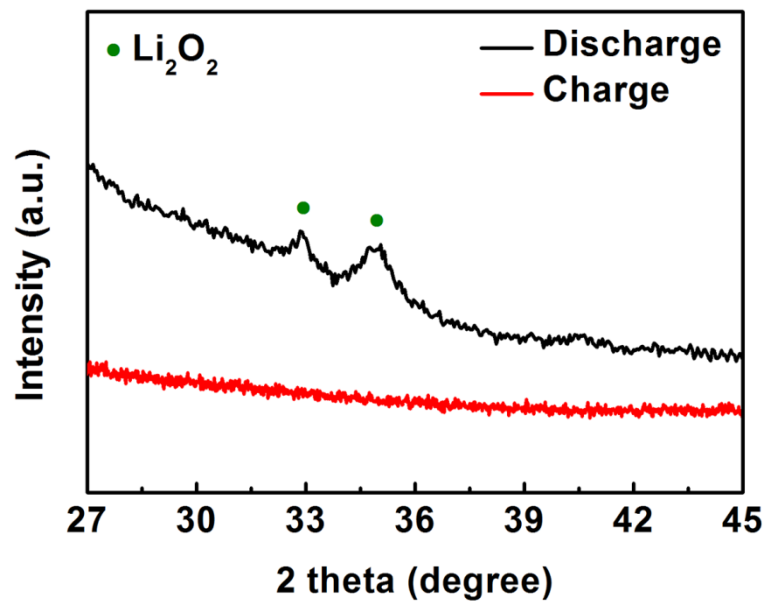


Figure S13. XRD patterns of the air electrode after the 300th (a) discharging and (b) recharging in ambient air with LDPE and LiI.

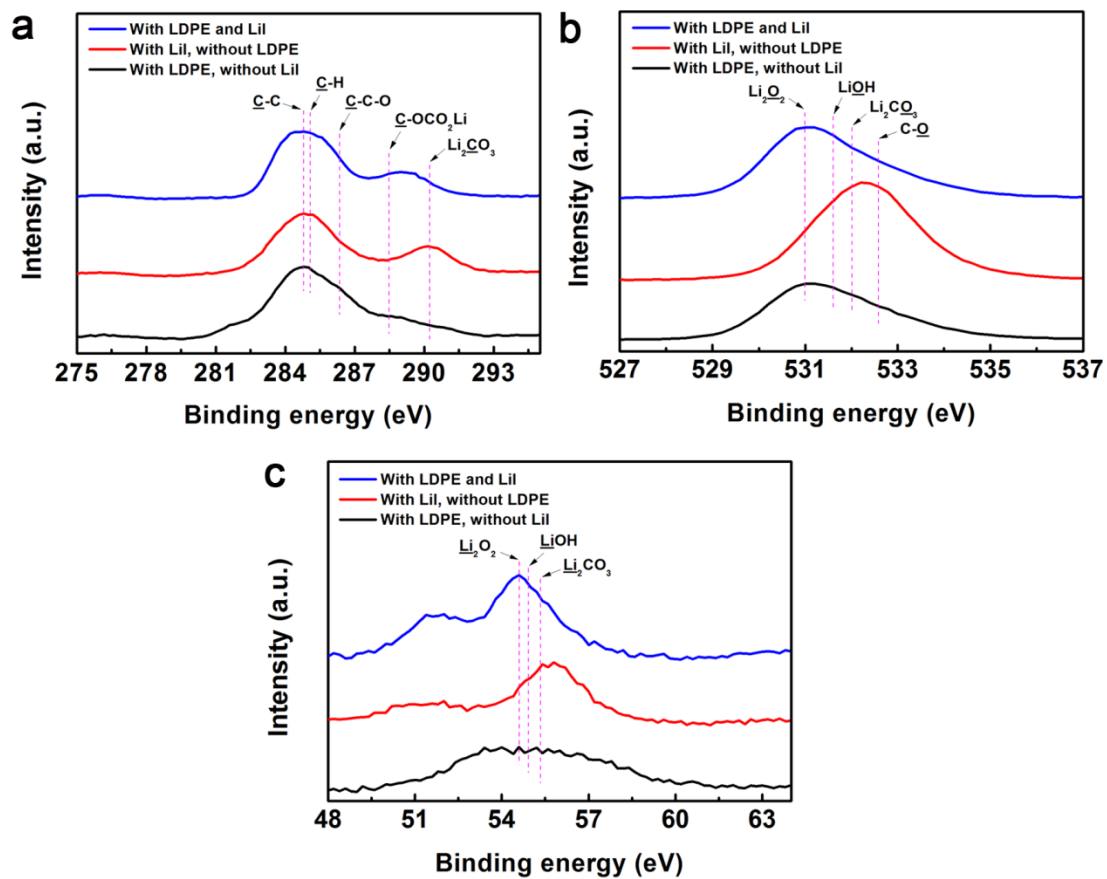


Figure S14. XPS characterizations of (a) C1s, (b) O1s and (c) Li1s signals of the air electrode after discharging in ambient air under different conditions.

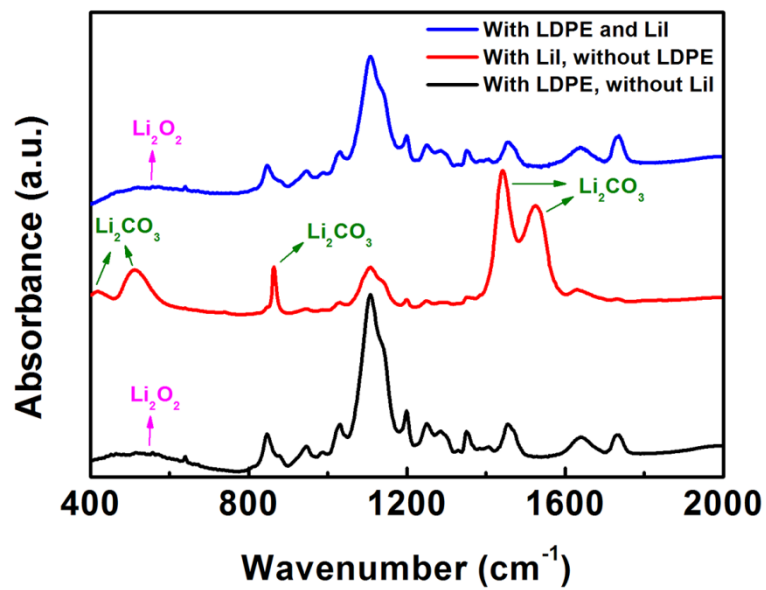


Figure S15. FTIR spectra of the air electrode after discharging in ambient air under different conditions.

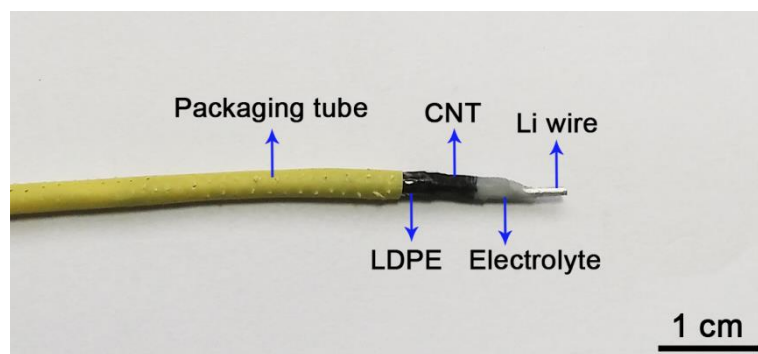


Figure S16. Photograph of a flexible fiber-shaped Li-air battery.

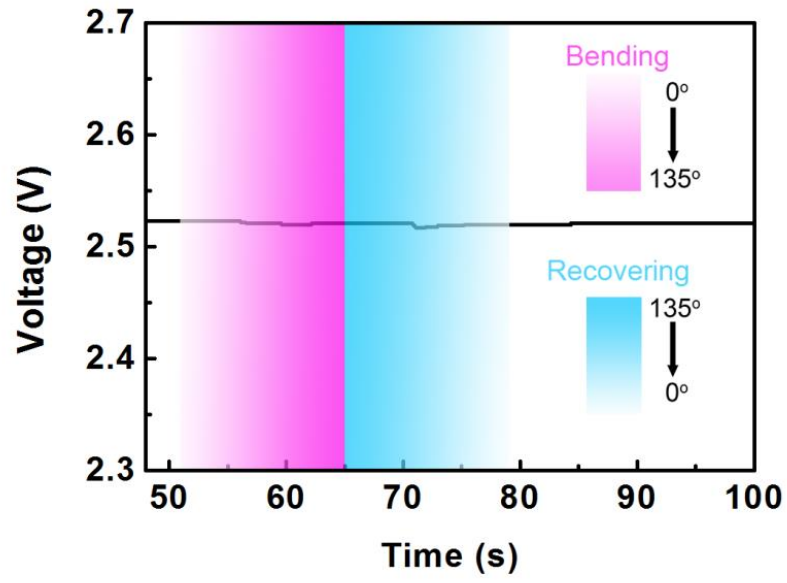


Figure S17. Discharge curve under a dynamic bending and recovering process.

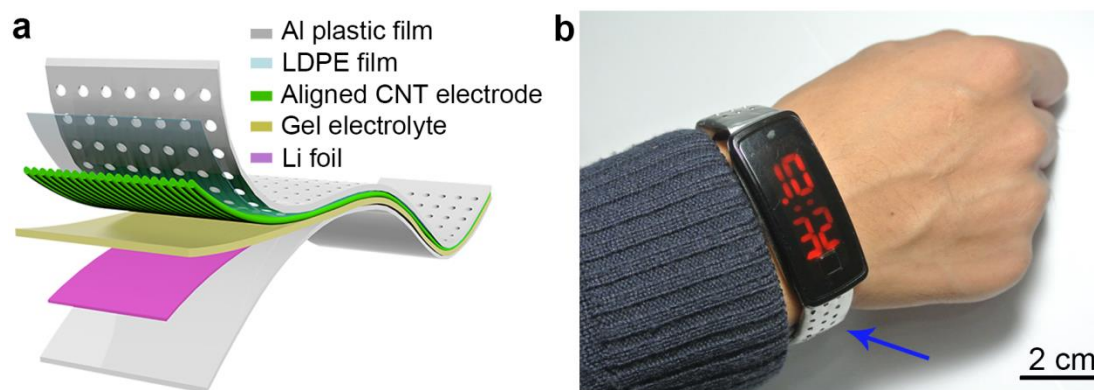


Figure S18. **a)** Multi-layered structure of the flexible strap-shaped Li-air battery. **b)** Photograph of a commercial LED watch powered by a strap-shaped Li-air battery. Blue arrows indicate the Li-air battery.

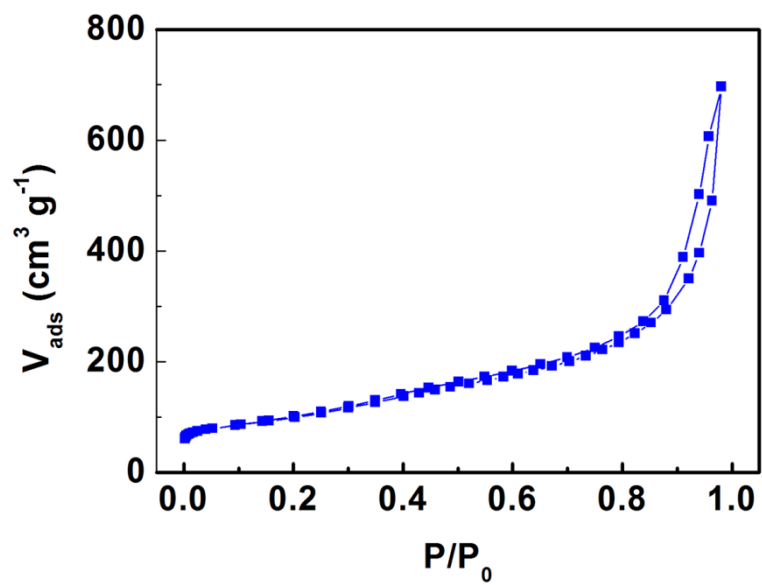


Figure S19. N_2 adsorption isotherms of the CNT air electrode.

Table S1. O₂ and H₂O permeability values of the LDPE film compared to the previous reports.

Material	O ₂ permeability (Barrer)	H ₂ O permeability (g m ⁻² d ⁻¹)	Ref.
LDPE film	40.26	0.825	This work
Silicon oil loaded PVDF-HFP	0.487	28.875	1
PVDF-HFP	0.021	811.997	2
PVDF-HFP-NS	3.147	11.160	
CAU-1-NH ₂ @PDA- PMMA	627.2	/	3
ML	0.02	/	4

Supporting References:

1. J. Amici, C. Francia, J. Zeng, S. Bodoardo, N. Penazzi, *J. Appl. Electrochem.* **2016**, *46*, 617.
2. J. Amici, M. Alidoost, C. Francia, S. Bodoardo, S. Martinez Crespiera, D. Amantia, M. Biasizzo, F. Caldera, F. Trotta, *Chem. Commun.* **2016**, *52*, 13683.
3. L. Cao, F. Lv, Y. Liu, W. Wang, Y. Huo, X. Fu, R. Sun, Z. Lu, *Chem. Commun.* **2015**, *51*, 4364.
4. J. Zhang, D. Wang, W. Xu, J. Xiao, R.E. Williford, *J. Power Sources* **2010**, *195*, 4332.